PHYSICAL REVIEW D VOLUME 10, NUMBER 5 1 SEPTEMBER 1974

# Nuclei as generators of quasireal photons: Testing an equivalent-photon method for calculating invariant-mass spectra*

C. Carimalo, G. Cochard, P. Kessler, J. Parisi, and B. Roehner
*Laboratoire de Physique Corpusculaire, Collège de France, Paris, France*

(Received 21 January 1974)

It is shown that the equivalent-photon method (Williams-Weizsäcker method) can be used to predict, with a good approximation, the invariant-mass spectra produced in various processes of inelastic scattering of high-energy nonhadronic particles (photons, charged leptons, neutrinos) in the electromagnetic field of nuclear targets. The test cases here considered are $\gamma+\mathfrak{N}\to\mu+\bar{\mu}+\mathfrak{N}'$, $\mu+\mathfrak{N}\to\mu+\gamma+\mathfrak{N}'$, $\mu+\mathfrak{N}\to\mu+\gamma^*+\mathfrak{N}'\to\mu+\mu+\bar{\mu}+\mathfrak{N}'$, and $\nu+\mathfrak{N}\to\mu+W+\mathfrak{N}'$. The nuclear targets involved in this study are ${}_1H^1$ and ${}_{92}U^{235}$. On the target side, both coherent scattering (in the case of uranium) and elastic plus inelastic scattering of individual nucleons are included in the calculations. For all four processes, both target nuclei and all partial contributions considered (as well as for the sum of these contributions), we compare the exact and the approximate values obtained for $d\sigma/dW$, where $W$ is the invariant mass of the system produced at the incident-particle vertex. A factorization formula, based on a helicity treatment, is used in the exact calculation; the equivalent-photon spectrum introduced is also derived from that formula.

## I. INTRODUCTION

The increasing importance of electromagnetic interactions, i.e., one-photon exchange processes, at growing accelerator energies has been stressed by many authors in the last years.[1-7]

One of the important aspects of the study of these interactions will be the search for any anomalies (such as heavy leptons or bosons) produced in the inelastic scattering of nonhadronic particles (photons, charged leptons, neutrinos) by the electromagnetic field of nuclei. It is thus useful to predict the invariant mass spectra produced in such processes, as given by the "normal" theory (QED or weak-interaction theory).

The equivalent-photon approximation (or Williams-Weizsäcker method[8]) has been used many times in the past (actually, from its very beginning) for computations of inelastic scattering processes in the Coulomb field.[9] Current variants of this method were tested, more or less successfully, by some authors; in most cases, the comparison with the exact calculation was made for the total cross section. Recently, Kim and Tsai[10] tested the validity of an improved Williams-Weizsäcker approximation for calculating angular distributions in the production of lepton and boson pairs in the Coulomb field, restricting themselves, however, to small angles.

It is not trivial to extend the principle of the equivalent-photon approximation (i.e., treating "almost real" photons as real ones) to the calculation of invariant mass spectra. As will be seen in Sec. II of this paper, high invariant masses produced at the incident-particle vertex involve a rather large minimal four-momentum transfer, i.e., virtual photons quite far from their mass shell. On the other hand, as we shall show, target excitation can no longer be neglected, and one must generalize the equivalent-photon method in order to include it. Such a generalization has not been performed before, except in the recent work of Kim and Tsai.[10]

It is the purpose of this paper to show that, in spite of these difficulties, it is possible to use an equivalent-photon method, as a good approximation, in the calculation of invariant mass spectra. The advantage, then, of using such a method is considerable and hardly contestable. It lies perhaps not as much in the field of practical computations (since the exact calculation can usually be performed without major problems, at least in lowest-order perturbation theory, by using powerful modern computer techniques) as in the physical transparency of the formulas obtained. Furthermore, it leads to a kind of philosophy for the type of processes considered: Nuclei are treated (just as are high-energy electrons in accelerators or $e^-e^+$ storage rings) as generators of quasireal photons, allowing one to perform photon-photon, photon-charged lepton, and photon-neutrino collisions (and also, to a more restricted extent, photon-pion or photon-kaon collisions[1,11]).

Our problem, thus, is to try to reduce the scheme of Fig. 1(a)—where $A$ is the incident nonhadronic particle, $\mathfrak{N}$ is the target nucleus, and $\mathfrak{N}'$ is its final (unexcited or excited) state, and $B$ is the system of interest—to that of Fig. 1(b). By

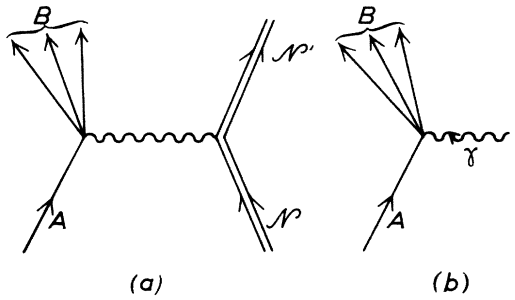


FIG. 1. Feynman diagrams for (a) $A+\mathfrak{N}\rightarrow B+\mathfrak{N}'$ via one-photon exchange; (b) $\gamma+A\rightarrow B$.

doing that, we are obviously neglecting two contributions:

(i) two-photon exchange, which might not be negligible, actually, in the case of high-$Z$ targets[12];

(ii) processes where $B$ is produced through excitation of the target (instead of excitation of $A$).[13]

Radiative corrections are also left out; scattering from atomic electrons, as well as screening, appear to be insignificant.

Four different effects (Fig. 2) are taken into account and summed up on the target side, in the general case of a complex nucleus:

(a) coherent elastic scattering,

(b) incoherent elastic scattering,

(c) incoherent inelastic scattering with resonance production,

(d) incoherent deep-inelastic scattering.

We here consider two different targets, uranium and hydrogen [for the latter, of course, "coherent" or "incoherent" becomes meaningless, and only the terms (b), (c), and (d) above are considered].

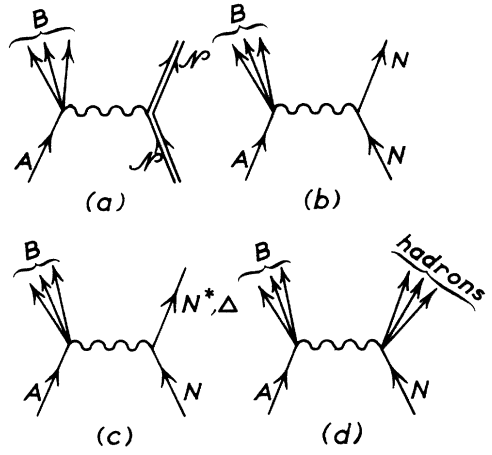


FIG. 2. Feynman diagrams for inelastic scattering in the electromagnetic field of nuclear targets. (a) Coherent elastic term; (b) incoherent elastic term; (c) incoherent inelastic (resonant) term; (d) incoherent deep inelastic term.

In the incoherent elastic term for the complex nucleus, restrictions due to the Pauli principle combined with the Fermi momentum distribution[14] are taken into account. On the other hand, the spread-out of the initial total energy, due to the Fermi motion inside the nucleus,[15] is neglected.

In Sec. II, we introduce a generalized helicity formula (demonstrated in Appendix A) for one-photon-exchange processes. This formula, involving a factorization of "virtual photoproduction" cross sections, provides by itself an important structural simplification. Actually, we use this formula in our exact calculations. On the other hand, it leads us in a very direct way—substituting a real photoproduction process for the virtual one at the incident-particle vertex—to an equivalent-photon approximation, involving further considerable simplifications. This approximation formula may be considered as a generalized Williams-Weizsäcker formula, since it allows one to include, in the most natural way, the "inelastic-inelastic" effects (i.e., inelastic also at the target vertex) in addition to the "elastic-inelastic" ones (elastic at the target vertex). Section II also contains the detailed expressions of the equivalent-photon spectra calculated in this formalism.

Section III shows the numerical comparison between both types of calculation (approximate and exact) for both target nuclei chosen, two energies of incident particles (20 and 200 GeV) and four different processes, namely (see Fig. 3):

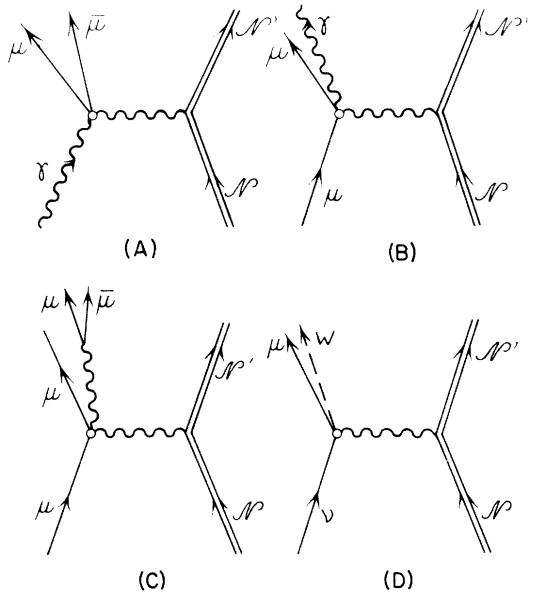


FIG. 3. Feynman diagrams for (A) $\gamma+\mathfrak{N}\rightarrow\mu+\bar{\mu}+\mathfrak{N}'$, (B) $\mu+\mathfrak{N}\rightarrow\mu+\gamma+\mathfrak{N}'$, (C) $\mu+\mathfrak{N}\rightarrow\mu+\gamma^*+\mathfrak{N}'\rightarrow\mu+\mu+\bar{\mu}+\mathfrak{N}'$, (D) $\nu+\mathfrak{N}\rightarrow\mu+W+\mathfrak{N}'$.

(A) $\gamma + \mathfrak{N} \rightarrow \mu + \bar{\mu} + \mathfrak{N}'$,

(B) $\mu + \mathfrak{N} \rightarrow \mu + \gamma + \mathfrak{N}'$,

(C) $\mu + \mathfrak{N} \rightarrow \mu + \gamma^* + \mathfrak{N}' \rightarrow \mu + \mu + \bar{\mu} + \mathfrak{N}'$

(where $\gamma^*$ is a timelike photon);

(D) $\nu + \mathfrak{N} \rightarrow \mu + W + \mathfrak{N}'$

(where $W$ is the intermediate vector boson of weak interactions). What is compared are the values—computed in both ways—of the differential cross sections with respect to the invariant mass of the system $B$ produced. The various contributions mentioned on the target side are considered first separately and then altogether. A detailed discussion is given on these numerical tests. The paper finishes with a short conclusion.

The expressions of the virtual photoproduction cross sections used—in the exact calculation—at the incident particle vertex, and those (usually much simpler) of the corresponding real photoproduction cross sections—used in the approximation—are shown in Appendix B.

## II. FORMALISM USED

In the framework of a generalized helicity method for Feynman-diagram calculations,[16] the following formula is established in Appendix A for any diagram involving one-photon exchange (Fig. 4):

$$\frac{d^3\sigma}{dt\,dW^2\,dW'^2} = \frac{1}{16\pi^3}\,\frac{(W^2-m^2)(W'^2-m'^2)}{\Lambda(s,m^2,m'^2)}\,\frac{1}{t^2}\left[\sigma_T\sigma'_T(1+\cosh^2\theta)+(\sigma_T\sigma'_L+\sigma_L\sigma'_T)\sinh^2\theta+\sigma_L\sigma'_L\cosh^2\theta\right], \tag{2.1}$$

where $t$ is the absolute value of the virtual photon's four-momentum squared; $s$ is the total energy squared (in the c.m. frame); $m, m'$ are the masses of the initial particles $A$ and $C$, respectively; $W, W'$ are the invariant masses of the final systems $B$ and $D$, respectively; $\Lambda$ is defined by

$$\Lambda(x,y,z) = x^2+y^2+z^2-2xy-2yz-2zx\,,$$

$\sigma_T, \sigma_L$ ($\sigma'_T, \sigma'_L$) are the usual "virtual photoproduction" cross sections,[17] transverse and longitudinal, at the left-hand (right-hand) vertex; and finally, $\theta$ is the "space-time rotation angle" between the left-hand and the right-hand "vertex plane" in four-space (see Appendix A).

From the exact formula (2.1), we derive the equivalent-photon approximation through the assumption (which is made implicitly or explicitly, in all equivalent-photon methods; see Ref. 18):

$$\sigma_T(W^2,t) \simeq \sigma_T(W^2,0) \equiv \sigma_\gamma(W^2)\,, \tag{2.2}$$

$$\sigma_L(W^2,t) \simeq \sigma_L(W^2,0) \equiv 0\,, \tag{2.3}$$

where $\sigma_\gamma$ is the free photoproduction cross section for $\gamma + A \rightarrow B$ (we always assume $B \neq A$), and where the identity used in the second line is due to gauge invariance.

Using this approximation, and defining an equivalent-photon spectrum $P(W)$ such that

$$\frac{d\sigma}{dW} \simeq P(W)\,\sigma_\gamma(W)\,, \tag{2.4}$$

we get from (2.1)

$$P(W) = \frac{W(W^2-m^2)}{8\pi^3\Lambda(s,m^2,m'^2)}\int\frac{W'^2-m'^2}{t^2}\left[\sigma'_T(1+\cosh^2\theta)+\sigma'_L\sinh^2\theta\right]dt\,dW'^2\,, \tag{2.5}$$

where the exact kinematic limits are used in the integration over $t$ and also (when the right-hand vertex is inelastic) over $W'^2$.

Coming back now to Fig. 2, we determine the various components of $P(W)$, i.e., we express $\sigma'_T, \sigma'_L$ for each of the contributions (a)–(d) occurring at the right-hand vertex [the same expressions are of course also used in the exact calculation, based on formula (2.1)].

*(a) Coherent elastic term.* As usual (except for the lightest nuclei), only the electric (Coulomb) term is included, and one thus gets

$$\sigma'_T = 0\,, \tag{2.6}$$

$$\sigma'_L = 16\pi^2\alpha Z^2F^2(t)\,m'^2(W'^2-m'^2)^{-1}\,\delta(W'^2-m'^2)\,, \tag{2.7}$$

where $m'$ is the full mass of the nucleus. The

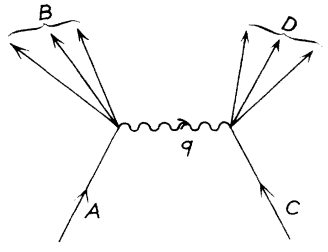


FIG. 4. Feynman diagram for $A + C \rightarrow B + D$ via one-photon exchange.

infinite factors $(W'^2-m'^2)^{-1}$ and $\delta(W'^2-m'^2)$ are obviously fictitious, since they drop out when $\sigma_L'$ is multiplied by external factors, integrated over $W'^2$. The electric form factor of $_{92}U^{235}$ is taken as follows[19]:

$$F(t)=\left(1+\frac{t}{0.011}\right)^{-2} \quad (t \text{ in GeV}^2/c^2). \tag{2.8}$$

*(b) Incoherent elastic term.* We get

$$\sigma_T'=4\pi^2\alpha t\,\mu^2G^2(t)R(t)(W'^2-m'^2)^{-1}\,\delta(W'^2-m'^2), \tag{2.9}$$

$$\sigma_L'=16\pi^2\alpha m'^2zG^2(t)R(t)(W'^2-m'^2)^{-1}\,\delta(W'^2-m'^2), \tag{2.10}$$

where $m'$ is now the nucleon's mass. Here again, the infinite factors drop out when multiplied by external factors, integrated over $W'^2$. $\mu$ is the magnetic moment of the nucleon (2.79 for the proton, $-1.91$ for the neutron) and $z$ is its charge (1 for $p$, 0 for $n$). The form factor $G(t)$ is taken as

$$G(t)=\left(1+\frac{t}{0.71}\right)^{-2} \quad (t \text{ in GeV}^2/c^2). \tag{2.11}$$

For a complex nucleus, the reduction factor $R(t)$, due to the Pauli principle combined with the Fermi momentum distribution, is given by[18]

$$R(t)=\frac{3}{4}\frac{\bar{t}^{1/2}}{Q_F}-\frac{1}{16}\frac{\bar{t}^{3/2}}{Q_F^3}, \quad \text{for } \bar{t}^{1/2}<2Q_F \tag{2.12}$$

$$R(t)=1, \quad \text{for } \bar{t}^{1/2}>2Q_F \tag{2.13}$$

where $\bar{t}=t+t^2/4m'^2$; for $Q_F$ (dimension of the Fermi sphere), we take the value 0.26 GeV.[20]

For elastic scattering on hydrogen, $\sigma_T'$ and $\sigma_L'$ are given by the same formulas with $R(t)\equiv 1$.

*(c) Incoherent inelastic (resonant) term.* We here consider the resonances $\Delta(1236)$, $N^*(1520)$, $N^*(1688)$. Using electroproduction and photoproduction data,[21] we take

$$\sigma_L'\simeq 0, \tag{2.14}$$

$$\sigma_T'\simeq\sigma_0\,\frac{W_0'^2\Gamma^2}{(W'^2-W_0'^2)^2+W_0'^2\Gamma^2}\,\phi(t), \tag{2.15}$$

where $W'$ is the on-shell mass of the resonance considered; $\sigma_0$ is the total photoproduction cross section at the mass $W'$; $\Gamma$ is the resonance width; $\phi(t)$ is a "virtuality factor" which we express by

$$\phi(t)=\left(1+\frac{t}{t_0}\right)^{-2}. \tag{2.16}$$

From the literature,[21] we extract the following values for the phenomenological parameters used:

| $W_0'$ (GeV) | 1236 | 1520 | 1688 |
|---|---|---|---|
| $\sigma_0$ ($\mu$b) | 600 | 300 | 250 |
| $t_0$ (GeV$^2/c^2$) | 2.5 | 3.0 | 3.0 |
| $\Gamma$ (GeV) | 0.15 | 0.15 | 0.15 |

We here make the assumption (roughly confirmed at least by experimental data on real photoproduction[22]) that the contribution is about the same for a neutron as for a proton target.

*(d) Incoherent deep-inelastic term.* Our calculations are based on the extensive analysis, performed by Brasse *et al.*,[23] of deep-inelastic electroproduction data (combined with photoproduction data). We thus use for a proton target

$$\sigma_L'=\frac{t}{\nu^2}\,\sigma_T', \tag{2.17}$$

$$\sigma_T'=\frac{4\pi^2\alpha}{W'^2-m'^2}\,\omega_W\sum_{n=3}^{7}b_n\left(1-\frac{1}{\omega_W}\right)^n, \tag{2.18}$$

where $m'$ is again the nucleon mass, and one defines

$$\nu=\frac{W'^2-m'^2+t}{2m'}, \tag{2.19}$$

$$\omega_W=\frac{2m'\nu+1.53}{t+0.41} \tag{2.20}$$

($W'$ and $m'$ being expressed in GeV, and $t$ in GeV$^2/c^2$), and $b_3=0.839$, $b_4=-1.398$, $b_5=8.985$, $b_6=-14.50$, $b_7=6.472$.

For a neutron target, we multiply the above-expressed cross sections by $(1+t/W'^2)^{-1}$ (see Ref. 24).

We let the deep-inelastic region start (as in Ref. 23) from $W'_{\min}=1.8$ GeV. The upper limit for $W'$ is $W'_{\max}=s^{1/2}-W$.

The contribution of the various incoherent terms (b), (c), and (d) to the over-all cross section is obviously obtained for complex nuclei by multiplying the proton cross section with the proton number ($Z$) and the neutron cross section with the neutron number ($A-Z$).

Finally, in all the calculations of partial equivalent-photon spectra [or partial contributions to the exact differential cross section, as expressed by formula (2.1)], we use

$$\sinh^2\theta=\frac{4st(t-t_{\min})(t_{\max}-t)}{\Lambda(W^2,m^2,-t)\Lambda(W'^2,m'^2,-t)}, \quad \cosh^2\theta=1+\sinh^2\theta, \tag{2.21}$$

$$t_{\max} = \frac{1}{2}\left[ s - \Sigma + \frac{(m'^2 - m^2)(W'^2 - W^2)}{s} + \frac{\Lambda^{1/2}(s, m^2, m'^2)\,\Lambda^{1/2}(s, W^2, W'^2)}{s} \right],$$
$$t_{\min} = \frac{1}{2}\left[ s - \Sigma + \frac{(m'^2 - m^2)(W'^2 - W^2)}{s} - \frac{\Lambda^{1/2}(s, m^2, m'^2)\,\Lambda^{1/2}(s, W^2, W'^2)}{s} \right], \tag{2.22}$$

with $\Sigma = m^2 + m'^2 + W^2 + W'^2$. (Let us recall that $m'$ is the mass of the nucleus in the coherent term, and that of the nucleon in the incoherent ones; the value of $s$ is also quite different, of course, for coherent and incoherent scattering.)

The above-expressed parameters $t_{\max}$, $t_{\min}$ are as well the limits of integration over $t$. Let us remark that formula (2.22) is not very convenient to use for computing the crucial parameter $t_{\min}$, since one has to take the difference between two huge terms in order to get a usually rather small quantity. Therefore we use

$$t_{\max}\, t_{\min} = (W^2 - m^2)(W'^2 - m'^2) + \frac{(W'^2 - W^2 - m'^2 + m^2)(m^2 W'^2 - m'^2 W^2)}{s}, \tag{2.23}$$

and obtain $t_{\min}$ by dividing that expression by $t_{\max}$ as given in (2.22).

When the right-hand vertex is elastic ($W' = m'$), one simply gets

$$t_{\max}\, t_{\min} = \frac{m'^2 (W^2 - m^2)^2}{s}. \tag{2.24}$$

In the high-energy limit, one obtains

$$t_{\max} \simeq \frac{(s - m'^2)^2}{s}, \quad t_{\min} \simeq \frac{m'^2 (W^2 - m^2)^2}{(s - m'^2)^2} \quad [\text{term (a)}] \tag{2.25}$$

$$t_{\max} \simeq s, \quad t_{\min} \simeq \frac{m'^2 (W^2 - m^2)^2}{s^2} \quad [\text{term (b)}] \tag{2.26}$$

$$t_{\max} \simeq s, \quad t_{\min} \simeq \frac{(W'^2 - m'^2)(W^2 - m^2)}{s} \quad [\text{term (c)}] \tag{2.27}$$

The above expressions of $t_{\min}$ clearly show that the virtual photon spectrum involved becomes "more off shell" when the invariant mass $W$ produced becomes larger. On the other hand, the photon spectrum becomes "less off shell" when the incident energy is increased.

The formulas given in this section allow us to calculate $d\sigma/dW$ both in an exact way (once we know $\sigma_T, \sigma_L$ for the process considered) and in the equivalent photon approximation (once we know $\sigma_\gamma$). For the four processes studied here (Fig. 3), the expressions found for $\sigma_\gamma$, $\sigma_T$, and $\sigma_L$ are shown in Appendix B.

## III. NUMERICAL DATA, AND DISCUSSION

Tables I–VIII show the ratio $(d\sigma/dW)_{\text{approx}} / (d\sigma/dW)_{\text{exact}}$ at two incident beam energies (20 and 200 GeV) and at a series of $W$ values, for the four processes considered and for the various terms we have defined ["uncorrelated" or "correlated" in the incoherent elastic contributions means without or with the reduction factor $R(t)$].

Some general features appear in these tables:

(i) One notices that the approximation works somewhat better at 200 GeV than at 20 GeV. This fact is easily understood, since a higher energy implies a smaller minimal transfer, i.e., a larger proportion of photons which are almost real [see Eqs. (2.25)–(2.27)].

(ii) The coherent term gives the best values. This observation is also easy to understand, since the contributions of large $t$ values (i.e., of highly virtual photons) are destroyed to a very large extent by the sharp form factor of the nucleus.

(iii) As to the incoherent elastic terms, the approximation works better for the proton than for the neutron; the obvious explanation is that in the proton case we have a mixture of electric ($\sigma_L'$) and magnetic ($\sigma_T'$) contributions, whereas the neutron gives only a magnetic one [remember from (2.9) and (2.10) that $\sigma_T'$ contains an extra factor $t$ with respect to $\sigma_L'$]. On the other hand, the "uncorrelated" figures are better than the "correlated" ones (where the lowest $t$ values are cut away to a large extent). However, at the upper end of the $W$ spectrum, all four values obtained (for $p$ or $n$, correlated or uncorrelated) become almost identical, for the following reason: Large $W$ values imply large $t$ values [since one has $t_{\min} \sim (W^2 - m^2)^2$]; the magnetic term then becomes largely predominant in the proton case too, and on the other hand the correlation plays no role any more.

(iv) For the resonant term, the approximation is, generally speaking, somewhat worse than for the incoherent elastic ones; and for the deep-inelastic terms, it is still worse. These facts are easily understood, since larger $t$ values are involved when the inelasticity at the right-hand vertex becomes higher [see Eq. (2.27)].

Apart from these common features, each process considered shows some particular characteristics.

For process (A), the approximation appears to

TABLE I. Ratio $R \equiv (d\sigma/dW)_{\text{approx}}/(d\sigma/dW)_{\text{exact}}$ for various contributions to the process $\gamma + \mathfrak{N} \to \mu + \bar{\mu} + \mathfrak{N}'$ at beam energy $E_\gamma = 20$ GeV.

| $W_{\mu\bar{\mu}}$ (GeV) | U coherent | $p$ elastic (uncorrelated) | $n$ elastic (uncorrelated) | $p$ elastic (correlated) | $n$ elastic (correlated) | $p,n$ resonant | $p$ deep-inelastic | $n$ deep-inelastic |
|---|---|---|---|---|---|---|---|---|
| 0.22 | 1.001 | 1.005 | 1.036 | 1.019 | 1.049 | 1.039 | 1.063 | 1.062 |
| 0.3 | 1.001 | 1.010 | 1.070 | 1.037 | 1.095 | 1.078 | 1.158 | 1.157 |
| 0.5 | 1.001 | 1.010 | 1.050 | 1.028 | 1.065 | 1.062 | 1.137 | 1.138 |
| 1.0 | 1.001 | 1.017 | 1.056 | 1.033 | 1.069 | 1.085 | 1.190 | 1.191 |
| 2.0 | 0.997 | 1.023 | 1.044 | 1.030 | 1.051 | 1.102 | 1.271 | 1.267 |
| 3.0 | 0.992 | 1.028 | 1.040 | 1.030 | 1.041 | 1.117 | 1.314 | 1.304 |
| 4.0 | 0.986 | 1.047 | 1.049 | 1.047 | 1.049 | 1.159 | 1.382 | 1.372 |

work particularly well, because of the special dynamics of the photoproduction of pairs: A factor $(W^2+t)^{-2}$ occurs at the left-hand vertex, i.e., in $\sigma_T, \sigma_L$ (see Appendix B); this factor plays the role of a form factor, i.e., cuts the larger $t$ values off to a large extent. One also notices that here the quality of the approximation does not depend strongly on $W$.

As to process (B), one remarks that the approximation is by far not as good as for (A). On the other hand, it is considerably worse here at the lowest $W$ values than at the higher ones. The explanation is the following:

When $W$ goes to its lower limit ($m$), the kinematic situation at the left-hand vertex becomes that of elastic scattering, where—as is well known—the equivalent-photon approximation cannot be applied any more. More precisely, for $W = m$ and $t$ finite, the exact calculation gives an infinite cross-section value (infrared divergence) whereas the approximation gives zero [because of the factor $(W^2 - m^2)$ in the equivalent-photon spectrum and of the finite Thomson limit for Compton scattering].[25] The situation improves, but only gradually, when one departs from the infrared limit; the approximation underestimates the exact result all along the $W$ spectrum. Some values in the upper right-hand corners of Tables III and IV seem really catastrophic; however, it will be shown that these values have practically no weight when the comparison between the approximation and the exact calculation is made for the over-all cross section.

In process (C), the quality of the approximation is intermediate, as compared to the cases (A) and (B). We also notice that there may be an underestimation or an overestimation, according to the various terms and $W$ values considered. Since a deep connection exists between the dynamics of processes (B) and (C), we are not surprised to remark that here, as in (B), the ratio between the approximate and the exact result steadily increases—in the incoherent terms at least—with rising $W$.

In the weak-interaction process (D), the approximation works less well, generally speaking, than in the QED processes considered above. As in (C), it overestimates or underestimates, according to the various terms and $W$ values involved. All values of the ratio defined go down with increasing $W$; the decrease is particularly sharp for the incoherent terms. Because of the complicated dynamics of the process, this phenomenon is hard to analyze.

TABLE II. Ratio $R$ for various contributions to the process $\gamma + \mathfrak{N} \to \mu + \bar{\mu} + \mathfrak{N}'$ at $E_\gamma = 200$ GeV.

| $W_{\mu\bar{\mu}}$ (GeV) | U coherent | $p$ elastic (uncorrelated) | $n$ elastic (uncorrelated) | $p$ elastic (correlated) | $n$ elastic (correlated) | $p,n$ resonant | $p$ deep-inelastic | $n$ deep-inelastic |
|---|---|---|---|---|---|---|---|---|
| 0.22 | 1.001 | 1.003 | 1.036 | 1.020 | 1.049 | 1.045 | 1.051 | 1.051 |
| 0.3 | 1.001 | 1.007 | 1.069 | 1.037 | 1.093 | 1.076 | 1.116 | 1.115 |
| 0.5 | 1.000 | 1.006 | 1.050 | 1.028 | 1.065 | 1.051 | 1.091 | 1.090 |
| 1.0 | 1.000 | 1.009 | 1.055 | 1.030 | 1.068 | 1.063 | 1.122 | 1.121 |
| 2.0 | 1.000 | 1.009 | 1.040 | 1.021 | 1.049 | 1.056 | 1.156 | 1.153 |
| 3.0 | 1.000 | 1.007 | 1.026 | 1.013 | 1.031 | 1.041 | 1.159 | 1.155 |
| 4.0 | 1.000 | 1.006 | 1.017 | 1.009 | 1.021 | 1.031 | 1.155 | 1.150 |
| 5.0 | 1.000 | 1.005 | 1.012 | 1.007 | 1.014 | 1.025 | 1.150 | 1.144 |
| 6.0 | 1.000 | 1.004 | 1.008 | 1.005 | 1.009 | 1.021 | 1.145 | 1.138 |
| 8.0 | 1.000 | 1.004 | 1.006 | 1.005 | 1.006 | 1.017 | 1.135 | 1.128 |

TABLE III. Ratio $R$ for various contributions to the process $\mu + \mathfrak{N} \to \mu + \gamma + \mathfrak{N}'$ at $E_\mu = 20$ GeV.

| $W_{\mu\gamma}$ (GeV) | U coherent | $p$ elastic (uncorrelated) | $n$ elastic (uncorrelated) | $p$ elastic (correlated) | $n$ elastic (correlated) | $p,n$ resonant | $p$ deep-inelastic | $n$ deep-inelastic |
|---|---|---|---|---|---|---|---|---|
| 0.12 | 0.896 | 0.736 | 0.005 | 0.077 | 0.001 | 0.004 | 0.001 | 0.001 |
| 0.2 | 0.950 | 0.754 | 0.082 | 0.278 | 0.033 | 0.069 | 0.019 | 0.020 |
| 0.3 | 0.974 | 0.790 | 0.191 | 0.422 | 0.111 | 0.158 | 0.048 | 0.052 |
| 0.5 | 0.987 | 0.839 | 0.385 | 0.605 | 0.292 | 0.312 | 0.109 | 0.117 |
| 1.0 | 0.992 | 0.894 | 0.680 | 0.806 | 0.619 | 0.556 | 0.240 | 0.259 |
| 2.0 | 0.986 | 0.927 | 0.882 | 0.909 | 0.861 | 0.754 | 0.419 | 0.445 |
| 3.0 | 0.972 | 0.933 | 0.931 | 0.930 | 0.927 | 0.811 | 0.521 | 0.546 |
| 4.0 | 0.952 | 0.924 | 0.927 | 0.924 | 0.927 | 0.799 | 0.543 | 0.558 |

It is of course of more practical importance to check the approximation on the over-all cross sections, i.e., the sum of all contributions for a given target nucleus. Such a check obviously depends not only on the values shown in Tables I–VIII, but also on the relative weight of the various terms. This relative weight can be inferred from Figs. 5–10 [since there are great similarities between all these figures, two cases were left out, namely process (A) at 20 GeV and process (B) at 200 GeV].

In Figs. 5–10, $d\sigma/dW$ is given, as obtained from the exact calculation, per nucleon of the target nucleus. The four curves shown in each figure represent the coherent elastic term for uranium; the elastic term for hydrogen; the incoherent elastic term for uranium, including the reduction factor $R(t)$ and averaging over neutrons and protons; the incoherent inelastic term, i.e., the sum of the resonant and the deep-inelastic contribution, averaging again over neutrons and protons for the uranium target; we checked that practically the same curve is also valid for the inelastic term in the case of a hydrogen target.

The following features are shown in Figs. 5–10.

(i) The coherent term dominates, for the uranium target, up to $W \simeq 1.5$–2 GeV at incident beam energy $E = 20$ GeV, and up to $W \simeq 5$ GeV at $E = 200$ GeV; at larger $W$ values, it becomes rapidly negligible with respect to the incoherent contribution. [Notice that, in process (D) at 20 GeV, because of the relatively high threshold, the incoherent part of the cross section practically predominates from the start.]

(ii) Among the incoherent terms, for the heavy target, the inelastic term is predominant at 200 GeV, with respect to the elastic one, in the entire region considered except near threshold. At 20 GeV, it dominates at the lower $W$ values (except again close to threshold), and then falls down below the incoherent elastic contribution (obviously because of the less available phase space). The difference between both incoherent terms is never very large, except in process (D) at 200 GeV.

(iii) For hydrogen, the elastic contribution dominates (quite strongly in the lower part of the $W$ spectrum, and only mildly in its higher part) over the inelastic one, both at 20 and 200 GeV. The only exception is, here again, process (D) at 200 GeV, where the inelastic term becomes the larger one at $W > 4$ GeV.

According to these curves, we expect the over-

TABLE IV. Ratio $R$ for various contributions to the process $\mu + \mathfrak{N} \to \mu + \gamma + \mathfrak{N}'$ at $E_\mu = 200$ GeV.

| $W_{\mu\gamma}$ (GeV) | U coherent | $p$ elastic (uncorrelated) | $n$ elastic (uncorrelated) | $p$ elastic (correlated) | $n$ elastic (correlated) | $p,n$ resonant | $p$ deep-inelastic | $n$ deep-inelastic |
|---|---|---|---|---|---|---|---|---|
| 0.12 | 0.929 | 0.814 | 0.005 | 0.078 | 0.001 | 0.005 | 0.001 | 0.001 |
| 0.2 | 0.969 | 0.829 | 0.081 | 0.280 | 0.033 | 0.080 | 0.024 | 0.025 |
| 0.3 | 0.986 | 0.861 | 0.190 | 0.428 | 0.111 | 0.179 | 0.060 | 0.063 |
| 0.5 | 0.995 | 0.902 | 0.383 | 0.616 | 0.292 | 0.349 | 0.128 | 0.135 |
| 1.0 | 0.998 | 0.947 | 0.675 | 0.826 | 0.615 | 0.614 | 0.266 | 0.280 |
| 2.0 | 0.999 | 0.975 | 0.877 | 0.938 | 0.853 | 0.825 | 0.436 | 0.456 |
| 3.0 | 0.999 | 0.984 | 0.938 | 0.968 | 0.926 | 0.900 | 0.538 | 0.560 |
| 4.0 | 0.999 | 0.988 | 0.964 | 0.980 | 0.957 | 0.934 | 0.607 | 0.629 |
| 5.0 | 0.999 | 0.990 | 0.977 | 0.986 | 0.972 | 0.952 | 0.659 | 0.681 |
| 6.0 | 0.999 | 0.991 | 0.984 | 0.989 | 0.981 | 0.962 | 0.700 | 0.721 |
| 8.0 | 0.998 | 0.992 | 0.990 | 0.992 | 0.989 | 0.973 | 0.762 | 0.782 |

TABLE V. Ratio $R$ for various contributions to the process $\mu + \mathfrak{N} \to \mu + \gamma^* + \mathfrak{N}' \to \mu + \mu + \bar{\mu} + \mathfrak{N}'$ at $E_\mu = 20$ GeV.

| $W_{\mu\mu\bar{\mu}}$ (GeV) | U coherent | $p$ elastic (uncorrelated) | $n$ elastic (uncorrelated) | $p$ elastic (correlated) | $n$ elastic (correlated) | $p,n$ resonant | $p$ deep-inelastic | $n$ deep-inelastic |
|---|---|---|---|---|---|---|---|---|
| 0.32 | 0.994 | 0.952 | 0.638 | 0.818 | 0.511 | 0.599 | 0.372 | 0.383 |
| 0.4 | 0.993 | 0.936 | 0.626 | 0.797 | 0.518 | 0.578 | 0.349 | 0.362 |
| 0.5 | 0.994 | 0.936 | 0.663 | 0.816 | 0.571 | 0.605 | 0.363 | 0.377 |
| 1.0 | 0.998 | 0.981 | 0.888 | 0.952 | 0.849 | 0.813 | 0.512 | 0.537 |
| 2.0 | 0.976 | 1.040 | 1.060 | 1.050 | 1.060 | 1.050 | 0.753 | 0.788 |
| 3.0 | 0.937 | 1.090 | 1.140 | 1.100 | 1.140 | 1.160 | 0.906 | 0.938 |
| 4.0 | 0.929 | 1.180 | 1.210 | 1.180 | 1.210 | 1.210 | 0.961 | 0.981 |

all ratio (approximation/exact calculation) to be mainly determined, for the heavy target, by this ratio's value for the coherent contribution in the lower part of the $W$ spectrum, and by its values for the incoherent terms in the higher part. For hydrogen, we expect in general the elastic term to be the most influential one, especially in the low-$W$ region.

These predictions are confirmed by Tables IX–XVI showing the over-all ratio for both nuclei considered. One notices that, on the whole, the approximation works well, and systematically better at 200 GeV than at 20 GeV. The worst case, as expected, is that of the weak-interaction process (D); but even there the order of magnitude given by the approximation is not too bad, since the error ranges between +70% and −50%.

As already mentioned, the "catastrophic" values found in the right-hand upper corner of Tables III and IV (and also some rather bad values in the right-hand upper corner of Tables VII and VIII are not reflected in the over-all ratio. The explanation of this fact can be stated as follows: the over-all cross section is mainly determined by contributions which contain the photon's pole (appearing in the form of a $t^{-1}$ factor) and by kinematic regions which are not too far from that pole; these contributions and regions are precisely those for which the equivalent-photon approximation is applied successfully; thus "bad" terms, such as those mentioned, happen to be small terms.

We finally remark that, in all Tables IX–XVI, the over-all ratio (approximation/exact calculation) tends to become about the same, for both nuclei considered, at the upper end of the $W$ spectrum. This is easily understood, since in that region the incoherent contribution becomes predominant by far for complex nuclei; and since—as already mentioned—neutrons and protons there practically behave in the same way (magnetic contribution) and, on the other hand, the correlation between the nucleons vanishes, i.e., $R(t) = 1$.

## IV. CONCLUSION

We have shown that the equivalent-photon method can be applied with confidence, in the high-energy region considered, to provide approximate predictions for one-photon-exchange processes with nuclear targets, even when inelasticity is included on the target side. We may now extend this approximation to other electromagnetic or weak-interaction processes, and also of course to other target nuclei (with different form factors involved in the coherent contribution; see Ref. 19). Actual-

TABLE VI. Ratio $R$ for various contributions to the process $\mu + \mathfrak{N} \to \mu + \gamma^* + \mathfrak{N}' \to \mu + \mu + \bar{\mu} + \mathfrak{N}'$ at $E_\mu = 200$ GeV.

| $W_{\mu\mu\bar{\mu}}$ (GeV) | U coherent | $p$ elastic (uncorrelated) | $n$ elastic (uncorrelated) | $p$ elastic (correlated) | $n$ elastic (correlated) | $p,n$ resonant | $p$ deep-inelastic | $n$ deep-inelastic |
|---|---|---|---|---|---|---|---|---|
| 0.32 | 0.997 | 0.970 | 0.637 | 0.822 | 0.511 | 0.629 | 0.422 | 0.430 |
| 0.4 | 0.997 | 0.962 | 0.624 | 0.803 | 0.518 | 0.610 | 0.395 | 0.404 |
| 0.5 | 0.998 | 0.963 | 0.661 | 0.823 | 0.571 | 0.639 | 0.407 | 0.417 |
| 1.0 | 1.001 | 0.992 | 0.883 | 0.959 | 0.845 | 0.843 | 0.549 | 0.565 |
| 2.0 | 1.002 | 1.020 | 1.050 | 1.040 | 1.050 | 1.030 | 0.754 | 0.775 |
| 3.0 | 1.003 | 1.030 | 1.080 | 1.060 | 1.090 | 1.090 | 0.875 | 0.897 |
| 4.0 | 1.003 | 1.040 | 1.090 | 1.060 | 1.100 | 1.120 | 0.957 | 0.978 |
| 5.0 | 1.002 | 1.050 | 1.090 | 1.060 | 1.100 | 1.130 | 1.020 | 1.040 |
| 6.0 | 0.999 | 1.050 | 1.090 | 1.070 | 1.100 | 1.140 | 1.070 | 1.090 |
| 8.0 | 0.990 | 1.070 | 1.090 | 1.070 | 1.100 | 1.160 | 1.140 | 1.160 |

TABLE VII. Ratio $R$ for various contributions to the process $\nu+\mathfrak{N}\to\mu+W+\mathfrak{N}'$ at $E_\nu=20$ GeV (mass and magnetic moment of the $W$: $M_W=2$ GeV, $g_W=2$).

| $W_{\mu W}$ (GeV) | U coherent | $p$ elastic (uncorrelated) | $n$ elastic (uncorrelated) | $p$ elastic (correlated) | $n$ elastic (correlated) | $p,n$ resonant | $p$ deep-inelastic | $n$ deep-inelastic |
|---|---|---|---|---|---|---|---|---|
| 2.2 | 1.093 | 1.499 | 1.843 | 1.672 | 1.765 | 1.715 | 5.104 | 4.943 |
| 2.3 | 1.005 | 1.240 | 1.383 | 1.326 | 1.456 | 0.932 | 2.258 | 2.200 |
| 3.0 | 1.003 | 1.025 | 1.029 | 1.028 | 1.031 | 0.370 | 0.507 | 0.582 |
| 4.0 | 0.967 | 0.994 | 0.991 | 0.993 | 0.990 | 0.226 | 0.298 | 0.319 |

ly, an equivalent-photon spectrum may be calculated once and forever for any type of target nucleus ("photon generator"), and then be applied to any process of the kind considered in Fig. 1(a). The use of this method is obviously justified by its simplicity and physical transparency.

So far, we have checked our equivalent-photon approximation on the invariant mass spectrum produced at the incident-particle's vertex. In a further study, we will verify that the same method is also able to reproduce approximately the angular and energy distributions of outgoing particles in the lab frame.

To analyze a given experiment—in particular if one looks for some small effect, such as a breakdown of QED—it will of course always be preferable to perform the exact calculation (including radiative corrections and other diagrams which were neglected here), and also to use still more refined nuclear models.


## ACKNOWLEGMENTS

Two of us (P. K. and J. P.) wish to thank Professor Y. S. Tsai and Professor S. J. Brodsky for interesting discussions.


## APPENDIX A: DERIVATION OF THE GENERALIZED HELICITY FORMULA FOR ONE-PHOTON-EXCHANGE PROCESSES

Considering a Feynman diagram of the type shown in Fig. 4, we write its differential cross section, according to standard techniques, in the form

$$d\sigma=\frac{1}{2\Lambda^{1/2}(s,m^2,m'^2)}\,\frac{1}{t^2}\,I\,\frac{d^4q}{(2\pi)^4}\,, \tag{A1}$$

where $s$, $t$, $m$, $m'$, and $\Lambda$ are defined as in Sec. II; and

$$I=I_{\mu\nu}I'^{*\mu\nu}\,, \tag{A2}$$

$$I_{\mu\nu}=\frac{1}{n}\sum\int d\Gamma\, j_\mu j_\nu^*\,, \tag{A3}$$

$$I'^{*\mu\nu}=\frac{1}{n'}\sum{}'\int d\Gamma'\, j'^{*\mu}j'^{\nu}\,, \tag{A4}$$

where $j_\mu$ is the electromagnetic current at the left-hand (or right-hand) vertex; $d\Gamma$ is the Lorentz-invariant phase-space factor at the left-hand vertex [incorporating a factor $(2\pi)^{-3}(2p_0)^{-1}d^3p$ for each final particle, and a factor $(2\pi)^4\times\delta^4(p_A-p_B-q)$], and $d\Gamma'$ is similarly defined at the right-hand vertex; $\sum$ ($\sum'$) means summing over all polarization states of initial and final particles at the left-hand (right-hand) vertex, and $n$ ($n'$) is the number of initial polarization states at either vertex. Using

$$d^4q=\frac{1}{4\Lambda^{1/2}(s,m^2,m'^2)}\,dt\,dW^2\,dW'^2\,d\phi\,, \tag{A5}$$

where $W$, $W'$ are defined as in Sec. II, and $\phi$ is the virtual photon's azimuthal angle, we are led to

$$\frac{d^3\sigma}{dt\,dW^2\,dW'^2}=\frac{1}{64\pi^3}\,\frac{1}{\Lambda(s,m^2,m'^2)}\,\frac{1}{t^2}\,I\,. \tag{A6}$$

Let us now establish the helicity structure of $I$,

TABLE VIII. Ratio $R$ for various contributions to the process $\nu+\mathfrak{N}\to\mu+W+\mathfrak{N}'$ ($M_W=2$ GeV, $g_W=2$) at $E_\nu=200$ GeV.

| $W_{\mu W}$ (GeV) | U coherent | $p$ elastic (uncorrelated) | $n$ elastic (uncorrelated) | $p$ elastic (correlated) | $n$ elastic (correlated) | $p,n$ resonant | $p$ deep-inelastic | $n$ deep-inelastic |
|---|---|---|---|---|---|---|---|---|
| 2.2 | 1.013 | 1.172 | 2.553 | 1.609 | 3.065 | 1.673 | 9.005 | 8.701 |
| 2.3 | 1.009 | 1.075 | 1.317 | 1.190 | 1.465 | 0.966 | 2.232 | 2.222 |
| 3.0 | 1.007 | 1.003 | 0.997 | 1.017 | 1.022 | 0.517 | 0.819 | 0.865 |
| 4.0 | 1.003 | 0.998 | 0.994 | 0.996 | 1.003 | 0.491 | 0.653 | 0.660 |
| 6.0 | 1.001 | 0.997 | 0.992 | 0.987 | 0.985 | 0.460 | 0.511 | 0.514 |
| 8.0 | 0.997 | 0.996 | 0.991 | 0.989 | 0.987 | 0.383 | 0.427 | 0.458 |

TABLE IX. Over-all ratio $R \equiv (d\sigma/dW)_{\text{approx}}/(d\sigma/dW)_{\text{exact}}$ for the process $\gamma + \mathfrak{N} \to \mu + \bar{\mu} + \mathfrak{N}'$ at $E_\gamma = 20$ GeV.

| $W_{\mu\bar{\mu}}$ (GeV) | H | U |
|---|---|---|
| 0.22 | 1.006 | 1.001 |
| 0.3 | 1.015 | 1.002 |
| 0.5 | 1.019 | 1.002 |
| 1.0 | 1.033 | 1.005 |
| 2.0 | 1.054 | 1.069 |
| 3.0 | 1.061 | 1.073 |
| 4.0 | 1.076 | 1.087 |

using the helicity treatment already shown in Ref. 16. We first remark that the four-vectors of the left-hand vertex $(p_A, p_B, q)$ are forming a plane (the "left-hand vertex plane") in four-space; similarly, we define the "right-hand vertex plane" $(p_C, p_D, q)$.

We introduce a set of unit polarization four-vectors $(\epsilon_\parallel, \epsilon_0, \epsilon_1, \epsilon_2)$ associated with the left-hand vertex and defined as follows in four-space: $\epsilon_\parallel$ is parallel to $q$; $\epsilon_0$ belongs to the left-hand vertex plane and is orthogonal to $\epsilon_\parallel$; $\epsilon_2$ is orthogonal to both vertex planes; and $\epsilon_1$ is orthogonal to $\epsilon_\parallel$, $\epsilon_0$, and $\epsilon_2$. We then use the circular combinations $\epsilon_\pm = \mp(\epsilon_1 \pm i\epsilon_2)/\sqrt{2}$ and thus stay with another set of unit polarization four-vectors $(\epsilon_\parallel, \epsilon_0, \epsilon_+, \epsilon_-)$, all mutually orthogonal $(\epsilon_m^* \epsilon_n = \pm \delta_{mn})$. Although the definition of these vectors is completely invariant, it is particularly simple to represent them in the Breit frame of the left-hand vertex (where $q$ is along the $z$ axis):

$$\epsilon_\pm = \mp(1, \pm i, 0, 0),$$

TABLE X. Over-all ratio $R$ for the process $\gamma + \mathfrak{N} \to \mu + \bar{\mu} + \mathfrak{N}'$ at $E_\gamma = 200$ GeV.

| $W_{\mu\bar{\mu}}$ (GeV) | H | U |
|---|---|---|
| 0.22 | 1.004 | 1.001 |
| 0.3 | 1.008 | 1.001 |
| 0.5 | 1.013 | 1.001 |
| 1.0 | 1.024 | 1.002 |
| 2.0 | 1.029 | 1.004 |
| 3.0 | 1.040 | 1.008 |
| 4.0 | 1.038 | 1.020 |
| 5.0 | 1.038 | 1.032 |
| 6.0 | 1.036 | 1.037 |
| 8.0 | 1.032 | 1.040 |

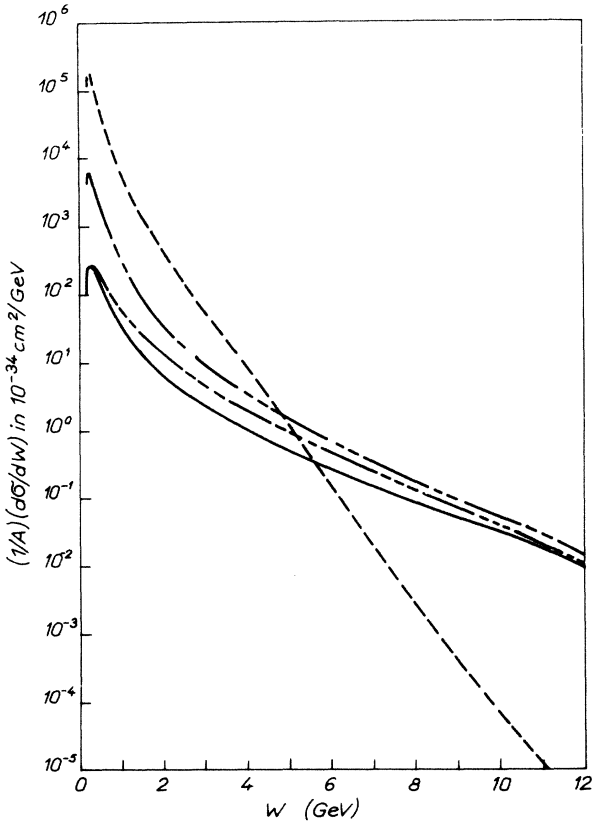


FIG. 5. Contributions to the $(\mu\bar{\mu})$ invariant mass spectrum produced, per target nucleon, in the reaction $\gamma + \mathfrak{N} \to \mu + \bar{\mu} + \mathfrak{N}$ at beam energy $E_\gamma = 200$ GeV. – – – U, coherent; ——— H, elastic; ——— U, incoherent elastic; ——— incoherent inelastic.

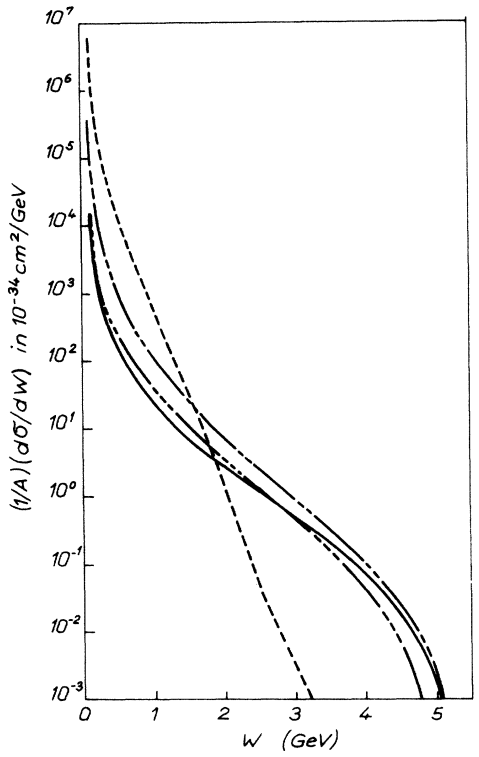


FIG. 6. Contributions to the $(\mu\gamma)$ invariant mass spectrum produced, per target nucleon, in the reaction $\mu + \mathfrak{N} \to \mu + \gamma + \mathfrak{N}'$ at beam energy $E_\mu = 20$ GeV. All curves are characterized as in Fig. 5.

TABLE XI. Over-all ratio $R$ for the process $\mu + \mathfrak{N} \to \mu + \gamma + \mathfrak{N}'$ at $E_\mu = 20$ GeV.

| $W_{\mu\gamma}$ (GeV) | H | U |
|---|---|---|
| 0.12 | 0.685 | 0.893 |
| 0.2 | 0.679 | 0.947 |
| 0.3 | 0.692 | 0.968 |
| 0.5 | 0.720 | 0.974 |
| 1.0 | 0.771 | 0.957 |
| 2.0 | 0.832 | 0.802 |
| 3.0 | 0.869 | 0.845 |
| 4.0 | 0.879 | 0.873 |

$$\epsilon_0 = \hat{1}(0, 0, 0, 1),$$

$$\epsilon_\parallel = (0, 0, 1, 0),$$

where the ordering of components is $(x, y, z, t)$ and where the factor $\hat{1}$ included in $\epsilon_0$ is the time-like unit, distinct from the imaginary unit $i$ ($\hat{1}^2 = -1$, but $\hat{1}^* = +\hat{1}$).

The physical interpretation of these polarization vectors is that $(\epsilon_0, \epsilon_+, \epsilon_-)$ are associated respectively with helicity states (helicity is here defined as the spin component in the vertex plane) $0, +1, -1$ of the virtual photon with respect to the left-hand vertex plane; $\epsilon_\parallel$ corresponds to the non-physical state of the photon ("scalar photon"). For the right-hand vertex, we introduce, in a similar way, a set of linear polarization vectors $(\epsilon'_\parallel, \epsilon'_0, \epsilon'_1, \epsilon'_2)$. Notice that $\epsilon'_\parallel \equiv \epsilon_\parallel$ and $\epsilon'_2 \equiv \epsilon_2$. We then make $\epsilon'_\pm = \mp(\epsilon'_1 \pm i\epsilon'_2)/\sqrt{2}$ and get another set $(\epsilon'_\parallel, \epsilon'_0, \epsilon'_+, \epsilon'_-)$.

The two tetrads $\epsilon_m$ and $\epsilon'_{m'}$, $(m, m' = \parallel, 0, +, -)$ can be superposed to each other by means of a four-space rotation made about the plane defined by $(\epsilon_\parallel, \epsilon_2)$ and carrying $(\epsilon_0, \epsilon_1)$ into $(\epsilon'_0, \epsilon'_1)$. The

TABLE XII. Over-all ratio $R$ for the process $\mu + \mathfrak{N} \to \mu + \gamma + \mathfrak{N}'$ at $E_\mu = 200$ GeV.

| $W_{\mu\gamma}$ (GeV) | H | U |
|---|---|---|
| 0.12 | 0.768 | 0.925 |
| 0.20 | 0.732 | 0.966 |
| 0.30 | 0.742 | 0.978 |
| 0.50 | 0.754 | 0.981 |
| 1.0 | 0.787 | 0.987 |
| 2.0 | 0.825 | 0.979 |
| 3.0 | 0.854 | 0.967 |
| 4.0 | 0.875 | 0.949 |
| 5.0 | 0.892 | 0.917 |
| 6.0 | 0.907 | 0.898 |
| 8.0 | 0.927 | 0.916 |

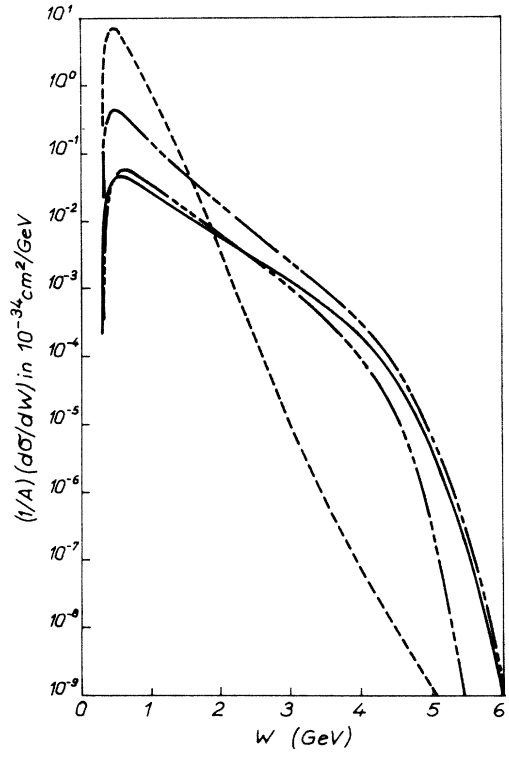


FIG. 7. Contributions to the $(\mu\mu\bar{\mu})$ invariant mass spectrum produced, per target nucleon, in the reaction $\mu + \mathfrak{N} \to \mu + \gamma^* + \mathfrak{N}' \to \mu + \mu + \bar{\mu} + \mathfrak{N}'$ at beam energy $E_\mu = 20$ GeV. All curves are characterized as in Fig. 5.

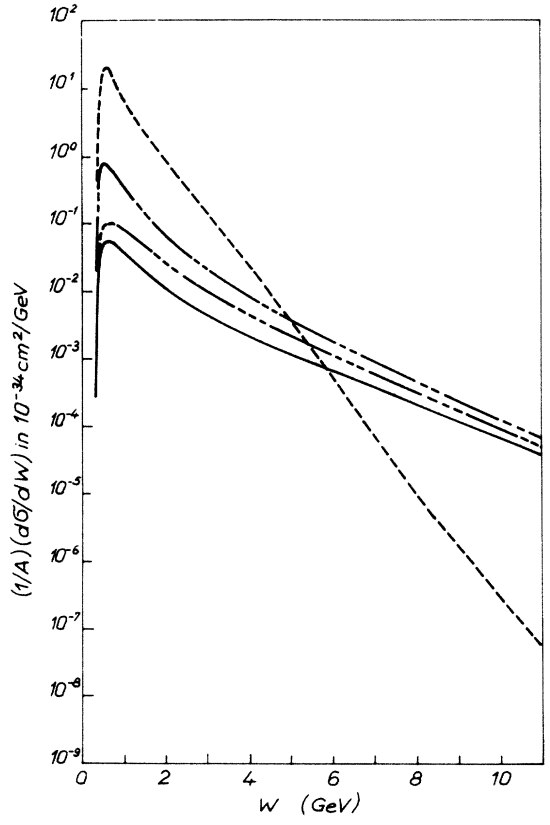


FIG. 8. Same contributions as in Fig. 7, at beam energy $E_\mu = 200$ GeV.

TABLE XIII. Over-all ratio $R$ for the process $\mu + \mathfrak{N} \to \mu + \gamma^* + \mathfrak{N}' \to \mu + \mu + \bar{\mu} + \mathfrak{N}'$ at $E_\mu = 20$ GeV.

| $W_{\mu\mu\bar{\mu}}$ (GeV) | H | U |
|---|---|---|
| 0.32 | 0.932 | 0.992 |
| 0.4 | 0.904 | 0.991 |
| 0.5 | 0.894 | 0.990 |
| 1.0 | 0.931 | 0.985 |
| 2.0 | 1.024 | 1.003 |
| 3.0 | 1.098 | 1.113 |
| 4.0 | 1.184 | 1.195 |

corresponding rotation matrix $[r_{mm'}]$ is defined by

$$\epsilon_m = \sum_{m'} r_{mm'} \epsilon'_{m'} \tag{A7}$$

and its expression is easily calculated (or derived from the Wigner rotation matrices, extrapolating them from real to imaginary rotation angles):

$$[r_{mm'}] = \begin{array}{c} m\backslash m' \\ + \\ 0 \\ - \\ \| \end{array} \begin{array}{c} \begin{array}{cccc} + & 0 & - & \| \end{array} \\ \begin{bmatrix} \frac{1+x}{2} & -\frac{y}{\sqrt{2}} & \frac{1-x}{2} & 0 \\ \frac{y}{\sqrt{2}} & x & -\frac{y}{\sqrt{2}} & 0 \\ \frac{1-x}{2} & \frac{y}{\sqrt{2}} & \frac{1+x}{2} & 0 \\ 0 & 0 & 0 & 1 \end{bmatrix} \end{array}, \tag{A8}$$

where $x = \cos\bar{\theta}$, $y = \sin\bar{\theta}$, $\bar{\theta}$ being the imaginary rotation angle.

Using the closure relation

$$g^{\mu\rho} = -\sum_m \epsilon^{*\mu}_m \epsilon^{\rho}_m \tag{A9}$$

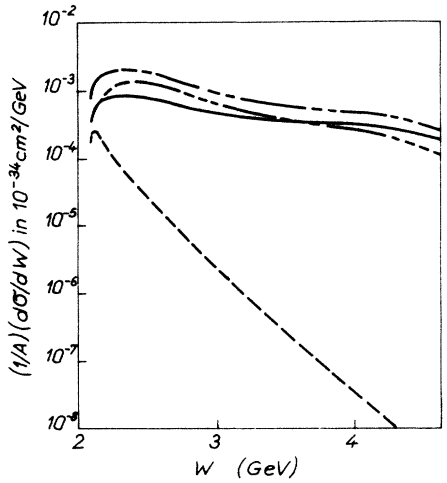


FIG. 9. Contributions to the $(\mu W)$ invariant mass spectrum produced, per target nucleon, in the reaction $\nu + \mathfrak{N} \to \mu + W + \mathfrak{N}'$ ($M_W = 2$ GeV, $g_W = 2$) at beam energy $E_\nu = 20$ GeV. All curves are characterized as in Fig. 5.

TABLE XIV. Over-all ratio $R$ for the process $\mu + \mathfrak{N} \to \mu + \gamma^* + \mathfrak{N}' \to \mu + \mu + \bar{\mu} + \mathfrak{N}'$ at $E_\mu = 200$ GeV.

| $W_{\mu\mu\bar{\mu}}$ (GeV) | H | U |
|---|---|---|
| 0.32 | 0.951 | 0.997 |
| 0.4 | 0.928 | 0.995 |
| 0.5 | 0.918 | 1.033 |
| 1.0 | 0.933 | 0.997 |
| 2.0 | 0.979 | 0.998 |
| 3.0 | 1.011 | 1.003 |
| 4.0 | 1.034 | 1.011 |
| 5.0 | 1.055 | 1.037 |
| 6.0 | 1.072 | 1.076 |
| 8.0 | 1.105 | 1.125 |

in combination with (A7), we immediately get

$$j_\mu j'^{*\mu} = j_\mu g^{\mu\rho} j'^*_\rho$$

$$= \sum_{m,m'} j_m \Gamma_{mm'} j'^*_{m'} \tag{A10}$$

defining

$$j_m = j_\mu \epsilon^{*\mu}_m, \quad j'_{m'} = j'_\rho \epsilon'^{*\rho}_{m'}, \tag{A11}$$

and we obtain

$$I = \sum_{m,m',n,n'} I_{mn} r_{mm'} r_{nn'} I'^*_{m'n'} \tag{A12}$$

defining

$$I_{mn} = I_{\mu\nu} \epsilon^{\mu}_m \epsilon^{*\nu}_n$$

$$= \frac{1}{n} \sum \int d\Gamma j_m j^*_n, \tag{A13}$$

$$I'_{m'n'} = I'_{\mu\nu} \epsilon'^{\mu}_{m'} \epsilon'^{*\nu}_{n'}$$

$$= \frac{1}{n} \sum \int d\Gamma j'_{m'} j'^*_{n'}. \tag{A14}$$

We notice that, in (A10) and (A12), only the values $m(m', n, n') = +, 0, -$ are to be considered, since $j_\parallel = j'_\parallel = 0$ by gauge invariance.

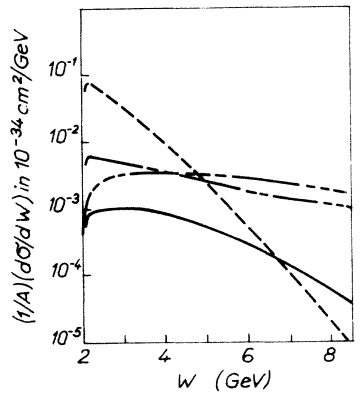


FIG. 10. Same contributions as in Fig. 9, at beam energy $E_\nu = 200$ GeV.

TABLE XV. Over-all ratio $R$ for the process $\nu + \mathfrak{N} \to \mu + W + \mathfrak{N}'$ ($M_W = 2$ GeV, $g_W = 2$) at $E_\nu = 20$ GeV.

| $W_{\mu W}$ (GeV) | H | U |
|---|---|---|
| 2.2 | 1.593 | 1.675 |
| 2.3 | 1.214 | 1.178 |
| 3.0 | 0.767 | 0.652 |
| 4.0 | 0.753 | 0.666 |

TABLE XVI. Over-all ratio $R$ for the process $\nu + \mathfrak{N} \to \mu + W + \mathfrak{N}'$ ($M_W = 2$ GeV; $g_W = 2$) at $E_\nu = 200$ GeV.

| $W_{\mu W}$ (GeV) | H | U |
|---|---|---|
| 2.1 | 1.317 | 1.034 |
| 2.3 | 1.157 | 1.023 |
| 3.0 | 0.851 | 0.967 |
| 4.0 | 0.790 | 0.891 |
| 6.0 | 0.702 | 0.600 |
| 8.0 | 0.636 | 0.548 |

In (A13), (A14), integration over the left-hand (right-hand) invariant phase space means that the left-hand (right-hand) final state may be decomposed into partial waves with well-defined quantum numbers: mass, spin, helicity, etc. It results that only diagonal density matrices are associated with the final (as well as the initial) states. This fact, together with rotational invariance (angular momentum conservation at either vertex), leads to the selection rule $n = m, n' = m'$; thus

$$I = \sum_{m,m'} I_m (\gamma_{mm'})^2 I'_{m'} , \tag{A15}$$

where we write $I_m$ for $I_{mm}$, and $I'_{m'}$ for $I'_{m'm'}$ ($\equiv I'^{*}_{m'm'}$). Using parity conservation ($I_+ = I_-$, $I'_+ = I'_-$), we get

$$I = I_+ I'_+ (1 + \cos^2\bar{\theta}) + (I_+ I'_0 + I_0 I'_+) \sin^2\bar{\theta} + I_0 I'_0 \cos^2\bar{\theta} . \tag{A16}$$

Then, using the conventional definition[17] of virtual (transverse and longitudinal) cross sections, i.e.,

$$\sigma_T = \frac{1}{2(W^2 - m^2)} I_+ , \quad \sigma_L = \frac{1}{2(W^2 - m^2)} (-I_0) , \tag{A17}$$

and substituting the resulting expression for $I$ in (A6), we get

$$\frac{d^3\sigma}{dt\, dW^2 dW'^2} = \frac{1}{16\pi^3} \frac{(W^2 - m^2)(W'^2 - m'^2)}{\Lambda(s, m^2, m'^2)} \cdots [\sigma_T \sigma'_T (1 + \cos^2\bar{\theta}) - (\sigma_T \sigma'_L + \sigma_L \sigma'_T) \sin^2\bar{\theta} + \sigma_L \sigma'_L \cos^2\bar{\theta}] . \tag{A18}$$

Since $\bar{\theta}$ is imaginary, we put $\cos\bar{\theta} = \cosh\theta$, thus $\sin^2\bar{\theta} = -\sinh^2\theta$, finally obtaining Eq. (2.1) of Sec. II. The calculation of $\cosh\theta$ or $\sinh\theta$, involving trivial kinematics, leads to Eq. (2.1).

A last remark: From (A13), using the helicity rule $m = n$ and the parity rule $I_+ = I_-$, together with (A9) and (A17), we are led to

$$\begin{aligned} I^{\mu\nu} &= \sum_m I_m \epsilon^{*\mu}_m \epsilon^{\nu}_m \\ &= I_0 \epsilon^{\mu}_0 \epsilon^{\nu}_0 + I_+ (\epsilon^{*\mu}_+ \epsilon^{\nu}_+ + \epsilon^{*\mu}_- \epsilon^{\nu}_-) \\ &= (I_0 - I_+) \epsilon^{\mu}_0 \epsilon^{\nu}_0 - I_+ (g^{\mu\nu} + \epsilon^{\mu}_{\parallel} \epsilon^{\nu}_{\parallel}) \\ &= \frac{-1}{2(W^2 - m^2)} [(\sigma_L + \sigma_T) \epsilon^{\mu}_0 \epsilon^{\nu}_0 + \sigma_T (g^{\mu\nu} + \epsilon^{\mu}_{\parallel} \epsilon^{\nu}_{\parallel})] . \end{aligned} \tag{A19}$$

Writing down the analogous expression for $I'_{\mu\nu}$, using (A2) and (A6), and making $\epsilon_0 \cdot \epsilon'_0 = -\cosh\theta$, we are brought back immediately to Eq. (2.1). On the other hand, noticing that $\epsilon^{\mu}_{\parallel} = q^{\mu}/(-q^2)^{1/2}$, and that $\epsilon^{\mu}_0$ can be expressed as

$$\epsilon^{\mu}_0 = \hat{1} \frac{2\sqrt{t}}{\Lambda^{1/2}(W^2, m^2, -t)} \left[ p^{\mu} - \frac{(p \cdot q)}{q^2} q^{\mu} \right] , \tag{A20}$$

where $p^{\mu} \equiv p^{\mu}_A$ or $p^{\mu}_B$, we may cast $I^{\mu\nu}$ into the familiar form

$$I^{\mu\nu} \sim W_2 p^{-2} \left[ p^{\mu} - \frac{(p \cdot q)}{q^2} q^{\mu} \right] \left[ p^{\nu} - \frac{(p \cdot q)}{q^2} q^{\nu} \right] \cdots - W_1 \left( g^{\mu\nu} - \frac{q^{\mu} q^{\nu}}{q^2} \right) , \tag{A21}$$

where $W_1$ and $W_2$ are the well-known structure functions,[26] related to the virtual photoproduction cross sections ($\sigma_T$ and $\sigma_T + \sigma_L$, respectively) by trivial proportionality factors. Thus the helicity treatment provides a better physical interpretation of the structure expressed by (A21).

## APPENDIX B: EXPRESSION OF $\sigma_T, \sigma_L, \sigma_\gamma$

We here give the expressions, for the processes (A)–(D) considered, of the virtual and real photoproduction cross sections for the left-hand vertex ($\gamma' + A \to B$, where $\gamma'$ is the spacelike photon exchanged, becoming real at the limit $t = 0$).

(A) $\gamma' + \gamma \to \mu + \bar{\mu}$.

$$\sigma^{(A)}_T = \frac{4\pi\alpha^2\beta W^2}{(W^2 + t)^2} \left[ \beta^2 - 2 + \frac{t}{2\mu^2}(1 - \beta^2) - \frac{t^2}{16\mu^4}(1 - \beta^2)^2 + \frac{3 - \beta^4 + (t^2/8\mu^4)(1 - \beta^2)^2}{2\beta} \ln\frac{1 + \beta}{1 - \beta} \right] , \tag{B1}$$

$$\sigma_L^{(A)}=\frac{16\pi\alpha^2\beta t}{(W^2+t)^2}\left[1-\frac{1-\beta^2}{2\beta}\ln\frac{1+\beta}{1-\beta}\right], \tag{B2}$$

$$\sigma_\gamma^{(A)}=\frac{4\pi\alpha^2\beta}{W^2}\left[\beta^2-2+\frac{3-\beta^4}{2\beta}\ln\frac{1+\beta}{1-\beta}\right], \tag{B3}$$

where $\mu$ is the muon mass, and $\beta=(1-4\mu^2/W^2)^{1/2}$.

(C) $\gamma'+\mu\to\mu+\gamma^*$. [We here consider (C) before (B), since the latter process may be treated as a limit case of the former one.]

$$\sigma_T^{(C)}=\frac{2\pi\alpha^2 q}{W(W^2-\mu^2)}\left\{\frac{I}{W^2-\mu^2}+\frac{W^2-\mu^2}{2kq}L+\frac{M^2+2\mu^2}{k^2}\left(2-\frac{L}{\rho}\right)\right.$$
$$\left.+\frac{2t}{W^2-\mu^2}\left[-\frac{2W^2+M^2}{W^2-\mu^2}-\frac{q}{k\rho}-(M^2+2\mu^2)I'+\frac{L}{2kq}\left(W^2+\mu^2+t-M^2+q^2-\frac{q^2}{\rho^2}\right)\right]\right\}, \tag{B4}$$

$$\sigma_L^{(C)}=\frac{2\pi\alpha^2 t q}{W^3(W^2-\mu^2)^2k^2}\left\{-W^2I+\frac{2}{(W^2-\mu^2)}\left[\mu^6-\mu^4(5W^2+M^2-t)-\mu^2(5W^4+4tW^2+tM^2)+W^4(W^2+t-3M^2)\right]\right.$$
$$+\frac{L}{2kq}\left[3\mu^6+2\mu^4(5W^2+3t)+\mu^2(3W^4+6W^2t-2W^2M^2+2t^2-2M^2t-M^4)\right.$$
$$\left.+M^2W^2(2W^2+2t-3M^2)\right]$$
$$\left.-2I'\left[4\mu^6+2\mu^4(2W^2+t-2M^2)-\mu^2M^2(t+M^2)-M^4(W^2+t-M^2)\right]\right\}, \tag{B5}$$

$$\sigma_\gamma^{(C)}=\frac{2\pi\alpha^2 q}{W(W^2-\mu^2)}\left[\frac{I_0}{W^2-\mu^2}+\frac{W^2-\mu^2}{2k_0q}L_0+\frac{M^2+2\mu^2}{k_0^2}\left(2-\frac{L_0}{\rho_0}\right)\right], \tag{B6}$$

where $M$ is the mass of the timelike photon $\gamma^*$, and

$$q=\frac{\Lambda^{1/2}(W^2,M^2,\mu^2)}{2W},\quad k=\frac{\Lambda^{1/2}(W^2,\mu^2,-t)}{2W},$$

$$I=\frac{1}{W^2}\left[(W^2-\mu^2)(W^2+\mu^2+t-M^2)+M^2t\right],$$

$$\rho=\frac{4kq}{I},\quad L=\ln\frac{1+\rho}{1-\rho},$$

$$I'=\frac{W^2(W^2-\mu^2)}{\mu^2(W^2-\mu^2)^2+tM^2(W^2+3\mu^2+t-M^2)},$$

$$k_0=\frac{W^2-M^2}{2W},$$

$$I_0=\frac{1}{W^2}\left[(W^2-\mu^2)(W^2+\mu^2-M^2)\right],$$

$$\rho_0=\frac{4k_0q}{I_0},\quad L_0=\ln\frac{1+\rho_0}{1-\rho_0},\quad I_0'=\frac{W^2}{\mu^2(W^2-\mu^2)}.$$

In these formulas, the heavy photon $\gamma^*$ is treated as a final particle. In order to account for the additional vertex $\gamma^*\to\mu+\bar{\mu}$ in process (C), the above given expressions for $\sigma_T^{(C)}, \sigma_L^{(C)}, \sigma_\gamma^{(C)}$ must be multiplied by the factor

$$\frac{2\alpha}{3\pi}\left(1-\frac{4\mu^2}{M^2}\right)^{1/2}\left(1+\frac{2\mu^2}{M^2}\right)\frac{dM}{M},$$

and integrated between $M_{\min}=2\mu$ and $M_{\max}=W-\mu$. Coming back now to process (B), i.e., $\gamma'+\mu\to\mu+\gamma$, we simply need to make

$$\sigma_T^{(B)}=\sigma_T^{(C)}(M=0),$$
$$\sigma_L^{(B)}=\sigma_L^{(C)}(M=0), \tag{B7}$$
$$\sigma_\gamma^{(B)}=\sigma_\gamma^{(C)}(M=0).$$

For $\sigma_\gamma^{(B)}$, it can be checked that one obtains the well-known Klein-Nishina formula.

(D) $\nu+\gamma'\to\mu+W$. With the value $g_W=2$ of the vector boson's magnetic moment, one gets for $\sigma_\gamma^{(D)}$

$$\sigma_\gamma^{(D)}=\frac{\alpha f^2}{2W^6M_W^2}\left\{4X(W^2-M_W^2+\mu^2)\left[W^4+(M_W^2-\mu^2)(2M_W^2+\mu^2)\right]\right.$$
$$+(2M_W^2+\mu^2)\left[2(M_W^2-3\mu^2)(W^2-M_W^2+\mu^2)-W^4\right]\ln\frac{1-X}{1+X}$$
$$\left.+2(2M_W^2+\mu^2)(M_W^2-\mu^2)(W^2-M_W^2-\mu^2)\ln\frac{1-Y}{1+Y}\right\}, \tag{B8}$$

where $f$ is the coupling constant of the $\nu\mu W$ vertex, $M_W$ the vector boson's mass, and

$$X=\frac{\Lambda^{1/2}(W^2,M_W^2,\mu^2)}{W^2-M_W^2+\mu^2},\quad Y=\frac{\Lambda^{1/2}(W^2,M_W^2,\mu^2)}{W^2+M_W^2-\mu^2}.$$

The corresponding formulas for $\sigma_T^{(D)}, \sigma_L^{(D)}$ are considerably longer than (B8), and actually too long to be given here. Notice that, when applying Eq. (2.1) or (2.5), one must make $m=0$ in process (A) or (D), and $m=\mu$ in process (B) or (C).

*Work partly supported by the Commissariat à l'Energie Atomique and by the DRME.

[1]L. Stodolsky, Phys. Rev. Lett. 26, 404 (1971); N. Jurisic and L. Stodolsky, Phys. Rev. D 3, 724 (1971); L. Stodolsky, J. Phys. (Paris) Suppl. 35, C2-87 (1974).

[2]M. Gourdin, Nucl. Phys. B32, 415 (1971).

[3]A. Dar, Proceedings of the VI Rencontre de Moriond, 1971 (unpublished); G. Berlad, A. Dar, G. Eilam, and J. Franklin, Ann. Phys. (N.Y.) 75, 461 (1973).

[4]F. Low and S. Treiman, Phys. Rev. D 5, 756 (1972).

[5]R. Nicot and Ph. Salin, Nucl. Phys. B38, 247 (1972).

[6]K. Fujikawa, Nuovo Cimento 12A, 117 (1972).

[7]S. G. Matinyan, N. L. Ter-Isaakyan, and V. A. Khoze, Zh. Eksp. Teor. Fiz. Pis'ma Red. 15, 110 (1972) [JETP Lett. 15, 76 (1972)]; S. G. Matinyan, N. L. Ter-Isaakyan, V. A. Khoze, and Yu.g. Shakhnazaryan, Yad. Fiz. 16, 793 (1973) [Sov. J. Nucl. Phys. 16, 440 (1973)].

[8]The semiclassical derivation of this method was given by E. J. Williams, Proc. R. Soc. A139, 163 (1933); Phys. Rev. 45, 729 (1934); K. Dan. Vidensk. Selsk. Mat.-Fys. Medd. 13, No. 4 (1935); C. F. von Weizsäcker, Z. Phys. 88, 612 (1934). See also: W. Heitler, *The Quantum Theory of Radiation*, 3rd edition (Clarendon, Oxford, 1953), p. 414; A. I. Akhiezer and V. B. Berestetskii, *Quantum Electrodynamics*, English edition (Interscience, New York, 1965), p. 473.

[9]For a general review of the equivalent-photon method, its applications and tests, see P. Kessler, J. Phys. (Paris) Suppl. 35, C2-97 (1974).

[10]J. K. Kim and Y. S. Tsai, Phys. Lett. 40B, 665 (1972); Phys. Rev. D 8, 3109 (1973).

[11]I. Ya. Pomeranchuk and I. M. Shmuskevitch, Nucl. Phys. 23, 452 (1961).

[12]See discussion of such corrections to Born-term calculations in: H. A. Bethe and L. C. Maximon, Phys. Rev. 93, 768 (1954); H. Davies, H. A. Bethe, and L. C. Maximon, *ibid.* 93, 788 (1954); S. J. Brodsky and J. R. Gillespie, *ibid.* 173, 1011 (1968); J. J. Russell *et al.*, Phys. Rev. Lett. 26, 46 (1971).

[13]In parton models [see, e.g., R. L. Jaffe, Phys. Rev. D 4, 1507 (1971)], one may speculate that such processes would actually give important contributions, at least for light nuclei and in some particular kinematic regions.

[14]J. S. Bell and M. Veltman, Phys. Rev. Lett. 5, 94 (1963).

[15]G. von Gehlen, Nuovo Cimento 30, 859 (1963). It appears there that the corresponding correction to the cross section, in the case of $\nu + \mathfrak{N} \to e + W + \mathfrak{N}$, is important only at energies close to the production threshold.

[16]P. Kessler, Cahiers de Physique 20, 55 (1966); Laboratoire de Physique Atomique Report No. PAM68-05, 1968 (unpublished); Nucl. Phys. B15, 253 (1970).

[17]L. N. Hand, Phys. Rev. 129, 1834 (1963).

[18]V. Gorge, M. Locher, and H. Rollnik, Nuovo Cimento 27, 928 (1963); V. Gorge, Nuovo Cimento 35, 545 (1965).

[19]This form factor was fitted *ad hoc* to the experimental data given by B. Hahn, D. G. Ravenhall, and R. Hofstadter, Phys. Rev. 101, 1131 (1966). In a preliminary version of our work [Laboratoire de Physique Corpusculaire Report No. LPC TH/74-02, 1974 (unpublished)], we considered two additional nuclei: carbon (with a harmonic square-well-type form factor), and cobalt (with a trapezoidal-type form factor). However, the conclusions obtained were basically similar to those shown here for the uranium target.

[20]H. Überall, *Electron Scattering from Complex Nuclei* (Academic, New York, 1971), p. 715.

[21]See J. Drees, in *Springer Tracts in Modern Physics*, edited by G. Höhler (Springer, New York, 1971), Vol. 60, p. 107.

[22]T. A. Armstrong *et al.*, Nucl. Phys. B41, 445 (1973).

[23]W. Brasse *et al.*, Nucl. Phys. B39, 421 (1972).

[24]H. W. Kendall, in *Proceedings of the 1971 International Symposium on Electron and Photon Interactions at High Energies*, edited by N. B. Mistry (Laboratory of Nuclear Studies, Cornell University, Ithaca, N. Y., 1972), p. 248.

[25]The reader may be somewhat puzzled by that statement, since the first application of the semiclassical Williams-Weizsäcker method was for the bremsstrahlung process, and there the infrared divergence appears in the approximation. The solution of this puzzle is the following: Whereas the divergent term is suppressed by extrapolating from the virtual to the real Compton scattering cross section (i.e., to the Thomson limit), the infrared divergence is reinduced, in the semiclassical formula, by an approximation involved in the quasireal photon spectrum. That approximation is equivalent, in our formalism, to substituting $(W^2 - m^2)^2$ for $\Lambda(W^2, m^2, -t)$ in the denominator of $\sinh^2\theta$ [Eq. (2.21)]. Using this substitution, the agreement in the low-$W$ region would certainly be improved substantially; however, for the coherence of the formalism, we preferred not to do so.

[26]S. D. Drell and J. D. Walecka, Ann. Phys. (N.Y.) 28, 18 (1964).